KMC Journal
[A Peer-Reviewed, Open-Access Multidisciplinary Journal]
ISSN 2961-1709 (Print)
Published by the Research Management Cell
Kailali Multiple Campus, Dhangadhi
Far Western University, Nepal
DOI: https://doi.org/10.3126/kmcj.v5i2.58241

First Principle Study on Structural, Electronic, Vibrational Properties and Molecular Docking Study of Tyramine

Govind Bahadur Dhami, Madhab Raj Bhatt, Shiv Raj Joshi, Bhawani Datt Joshi
Department of Physics, Siddhanath Science Campus, Mahendranagar (TU), Nepal
Corresponding Author: *Govind Bahadur Dhami;* Email: govind.755511@snsc.tu.edu.np

Abstract

First principle study of cyclic compound has a great interest because their products are very much useful in biological and clinical applications. In this work, Density functional theory (DFT) and Time dependent DFT calculations have been performed to study structural, electronic and vibrational properties of Tyramine (a neuromodulator) at B3LYP/3-21G level employing Gaussian 09 software. All the theoretical calculations were carried out to study the equilibrium geometries, vibrational spectra, molecular electrostatic potential (MEP), highest occupied molecular orbital (HOMO), lowest unoccupied molecular orbital (LUMO) and UV-Vis spectra of the title compound. Also, the molecular docking analysis of Tyramine against two different proteins (Trace amine-associated receptor 1 and Dopamine D_2 receptor) was carried out using AutoDock Vina. The scaled values of calculated vibrational frequencies were used for vibrational assignments on the basis of the potential energy distribution (PED). The structure activity relation has been interpreted by mapping MEP and Time dependent DFT method has been adopted to elucidate electronic properties. Graphical representation of frontier molecular orbital for both gaseous and solvent phase provides valuable insight into the nature of reactivity, stability and some of the structural and physical properties of the title molecule. Also, the calculated HOMO and LUMO energy values show that the charge transfer occurs within the molecule. Further, the title molecule shows good potentiality for binding against Trace amine-associated receptor 1 (1TQN) with binding affinity -6 kcal/mol The binding site of the Tyramine is found to be amine (NH_2) group.

Keywords: DFT, tyramine, spectroscopy, neuromodulator, binding affinity

Introduction

Trace amines, an endogenous group of trace amine-associated receptors 1 agonists, are monoaminergic neuromodulators (Burchett & Hicks, 2006; Lindemann & Hoener, 2005; Panas et al., 2012). They structurally and metabolically belong to the group of classical monoamine neurotransmitters (Broadely, 2010). Out of them, tyramine is a naturally occurring trace amine derived from tyrosine (Cruickshank et al., 2013). It is naturally found in animals, plants and foods and metabolized by monoamine oxidase (MOA) (Rafhei et ai., 2019; Salter & Kenney, 2018). Tyramine plays a role in animals in behavioral and motor function. And its abnormal level inside human body may cause problems like migraines, gastric, intestinal problem and allergic problem (Dong et al., 2022). It is also considered as a false neurotransmitter as it inters noradrenergic nerve terminal and displaces large amount of norepinephrine, which enters the blood stream and causes vasoconstriction. Tyramine is particularly important in medicinal chemistry and chemical biology. When tyramine is injected intravenously in the system, it causes relatively rapid and small release of a noradrenaline and thus producing the sympathomimetic effect (Podder et al. 1979).

Yadav and Mukherjee (2017) studied on structural modeling and spectroscopic investigation of isolated and hydrochloride tyramine neurotransmitter. Quevedo et al. (2012) worked on structural study of the intermolecular interactions of tyramine in the solid state and in solution. Also, Siddiqui et al. (2009) have published their paper on computational note on vibrational spectra of Tyramine hydrochloride: DFT study. Thus, Literature search show that none of the works have been reported covering completed theoretical study of tyramine including molecular docking. In this communication, we have adopted Density Functional Theory (DFT) / B3LYP/ 3-21G level of theory for molecular characterization. Structural, electronic and vibrational properties of the title compound have been addressed along with its molecular docking. The Raman (Crupi et al., 2002) and IR (Fini, 2002) spectra title molecule have been analyzed by DFT in terms of potential energy distribution (PED). Molecular electrostatic potential surfaces (MESP) has been plotted which is useful for understanding the relationship between molecular structure and biological activity. HOMO-LUMO plot made easier to understand the intramolecular charge transition property of the molecule. And, the molecular docking has been done to study binding mechanism of the title molecule with proteins. The optimized molecular structure of tyramine is given in the figure 1.

Figure 1

Optimized Molecular Structure of Tyramine

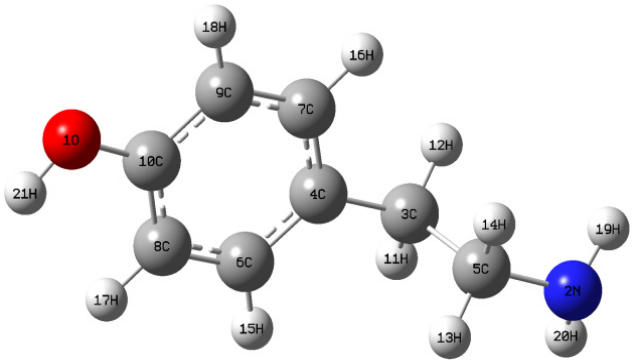

Methods and Procedures

As the first task of the study, geometry optimization was completed by using the geometrical parameters available from the PubChem database as the basis for the optimization. All the required calculations were carried out by using Density Functional Theory (DFT) (Chong, 1995; Hohenberg & Kohn, 1964). The geometry optimization and calculations of vibrational spectra were completed by using DFT/ B3LYP/ 3-21G level of theory employing Gaussian 09 program (Frisch et al., 2010) without any constraints on the geometry of molecule (Ullah et al., 2013). The basis set used for the calculations is based on Becke's three-parameter (local, non-local, Hartree-Fock) hybrid exchange functional with Lee-Yang-Parr correlation Functional (B3LYP) (Becke, 1993; Lee et al., 1988; Kohn & Bashishta, 1983).

After geometry optimization, the second task was calculation of vibrational modes and vibrational spectra using same level of theory. As the title molecule consists of 21 atoms, it has 57 normal modes of vibrations according to the relation, total modes of vibrations is 3N−6, (Misra et al., 2014) where, N represents total numbers of atoms. The normal modes of vibrational analysis were performed along with potential energy distribution (PED) calculations. The complete vibrational spectra were done by employing Gaussian 09 program without any constraints on geometry of molecule. Potential energy distribution (PED) was calculated using the internal coordinates of molecular geometry using localized symmetry. For this purpose, a complete set of 57 internal coordinates were defined using Pulley's recommendation (Pulay et al., 1979). Finally, vibrational assignment of all normal modes was made on the basis of the PED calculated by the program GAR2PED (Martin & Alsenoy, 1995). The visualization of calculated data was done by using the GaussView (Frish et al. 2009). The electronic absorption wavelength was calculated both in the solvent and gaseous phases by using time-dependent density functional

theory (TD−DFT) (Casida et al., 1998). For molecular docking, AutoDock Vina (Trott et al., 2010) has been employed for docking whereas AutoDock tools (Morris et al., 2009) were used for ligand and protein preparation. Finally, Biovia Discovery Studio (Systemes, 2016) and PyMOL (Schrodinger & PyMol, 2020) were used for the interaction visualization.

Results and Discussion

Geometry Optimization

The optimized structural parameters of tyramine calculated by DFT and B3LYP method with the 6-21G basis set are listed in Table 1. It includes bond length, bond angle and dihedral angle. The bond length is determined by the number of bonded electrons. The bond length between two atoms in a molecule depends not only depends on the atoms but also depends on factors as the orbital hybridization and the electronic and steric nature of the substituent. Higher the bond order (number of bonded electrons), stronger is the pull between atoms and shorter the bond length and vice-versa.

Table 1

Optimized Values of Bond Length, Bond Angles and Dihedral Angles of Tyramine

Optimized parameter					
Bond length(Å)		Bond Angle(°)		Dihedral Angle(°)	
Bond length	Optimized Value	Bond Angle	Optimized Value	Dihedral Angle	Optimized Value
R(O1–C10)	1.3884	A(C10 – O – H21)	109.8572	D(21H–O1–C10–C8)	0.1950
R(O1–H21)	0.9922	A(C5–N2–H19)	112.1374	D(21H–O1–C10–C9)	-179.9831
R(N2–C5)	1.4765	A(C5–N2–H20)	112.1463	D(19H–N2–C5–C5–3C)	62.1368
R(N2–H19)	1.0242	A(H19–N2–20H)	109.6532	D(19H–N2–C5–C5–C5–13H)	-175.8673
R(N2–H20)	1.0242	A(C4–C3–C5)	111.5374	D(19H–N2–C5–C5–C5–14H)	-59.8789
R(C3–C4)	1.5150	A(C4–C3–H11)	110.2131	D(20H–C5–N2–C5–C5–C5–3C)	-61.7524
R(C3–C5)	1.5618	A(C4–C3–H12)	110.1661	D(20H–C5–N2–C5–C5–C5–13H)	60.2435
R(C3–H11)	1.0978	A(C5–C3–H11)	108.5753	D(20H–C5–N2–C5–C5–C5–14H)	176.2319
R(C3–H12)	1.0978	A(C5–C3–H12)	108.565	D(5–C5–3C–C5–4C–C5–C6)	-88.7645
R(C4–C6)	1.3997	A(H11–C3–H12)	107.6798	D(5–C5–3C–C5–4C–C5–C7)	87.8469
R(C4–C7)	1.4042	A(C3–C4–C6)	121.1044	D(11H–C5–3C–C5–4C–C5–C6)	-32.7885

R(C5–H13)	1.0955	A(C3–C4–C7)	120.9696	D(11H–C5–3C–C5–4C–C5–C7)	-151.4727
R(C5–H14)	1.0954	A(C6–C4–C7)	117.8428	D(12H–C5–3C–C5–4C–C5–C6)	150.6000
R(C6–C8)	1.3952	A(N2–C5–C3)	115.2315	D(12H–C5–3C–C5–4C–C5–C7)	-32.7885
R(C6–H15)	1.0852	A(N2–C5–13H)	108.3968	D(4C–C5–3C–C5–C5–C5–N2)	-179.8424
R(C7–C9)	1.3902	A(N2–C5–14H)	108.3735	D(4C–C5–3C–C5–C5–C5–13)	58.3140
R(C7—H16)	1.0852	A(3C—C5 —13H)	108.6798	D(4C–C5–3C–C5–C5–C5–14H)	-58.0071
R(C8—C10)	1.3969	A(3C—C5 —14H)	108.7087	D(11H–C5–3C–C5–C5–C5–N2)	58.5235
R(C8—H17)	1.0857	A(13H—C5 —14H)	107.1647	D(11H–C5–3C–C5–C5–C5–13H)	-63.3200
R(C9—C10)	1.3991	A(4C—C6 —C8)	121.1967	D(11H–C5–3C–C5–C5–C5–14H)	-179.6412
R(C9—H18)	1.0820	A(4C—C6 —15H)	119.5176	D(12H–C5–3C–C5–C5–C5–N2)	-58.2741
		A(C8—C6 —15H)	119.2843	D(12H–C5–3C–C5–C5–C5–13H)	179.8824
		A(4C—C7 —C9)	121.3443	D(12H–C5–3C–C5–C5–C5–14H)	63.5612
		A(4C—C7 —16H)	119.3688	D(3C–C5–4C–C5–C6–C5–C8)	176.9745
		A(C9—C7 —16H)	119.2856	D(3C–C5–4C–C5–C6–C5–15H)	-3.4506
		A(C6—C8 —10)	120.2778	D(C7–C5–4C–C5–C6–C5–C8)	0.2602
		A(C6—C8—17H)	119.6688	D(C7–C5–4C–C5–C6–C5–15H)	179.8352
		A(C10—C8—17H)	120.0531	D(3C–C5–4C–C5–C7–C5–C9)	-176.9766
		A(C7—C9—C10)	120.2018	D(3C–C5–4C–C5–C7–C5–16H)	3.4488
		A(C7—C9—18H)	121.5177	D(C6–C5–4C–C5–C7–C5–C9)	-0.2577
		A(C10—C9—18H)	118.2802	D(C6–C5–4C–C5–C7–C5–16H)	-179.8323
		A(1O—C10—C8)	123.6529	D(4C–C5–C6–C5–C8–C5–C10)	-0.1686

A(1O—C10—C9)	117.2108	D(4C–C5–C6–C5–C8–C5–17H)	179.6246
A(C8—C10—C9)	119.1361	D(15H–C5–C6–C5–C8–C5–C10)	-179.7445
		D(15H–C5–C6–C5–C8–C5–17H)	0.0487
		D(C4–C5–C7–C5–C9–C5–C10)	0.1624
		D(4C–C5–C7–C5–C9–C5–18H)	-179.6325
		D(16H–C5–C7–C5–C9–C5–C10)	179.7374
		D(16H–C5–C7–C5–C9–C5–18H)	-0.0575
		D(C6–C5–C8–C5–C10–C5–O1)	179.8830
		D(C6–C5–C8–C5–C10–C5–C9)	0.0643
		D(17H–C5–C8–C5–C10–C5–O1)	0.0906
		D(17H–C5–C8–C5–C10–C5–C9)	-179.7281
		D(C7–C5–C9–C5–C10–C5–O1)	-179.8916
		D(C7–C5–C9–C5–C10–C5–C8)	-0.0614
		D(1C8–C5–C9–C5–C10–C5–1O)	-0.0902
		D(18H–C5–C9–C5–10–C5–C8)	179.7401

The CC single bond length is generally 1.54 Å, CH is 1.09 Å, C—O is 1.43Å, C=O is 1.23 Å, CN is 1.47 Å and that of N—H is 1.5-2.5 Å. Carbon-carbon bond lengths are known to vary from about 1.20 to 1.54 Å (Corminboeuf et al., 2006; Pauling, 1960) depending on the chemical nature of their bonding (Dewar, 1960. In this study, the longest C—C bond was found between C3—C5 and minimum between C7—C9 which are respectively 1.5618 Å and 1.3902 Å. From table it is clear that the calculated bond lengths are approximately in agreement with the experimental data. The bond angle depends upon repulsion between atoms or groups attached to the central atom may increase or decrease the bond angle. In hybridization as the s

character of the s hybrid bond increases, the bond angle increases and by increasing lone pair of electron, bond angle decreases approximately by 2.5%. Higher value of bond angle was found for 1O−C10−C8 which is 123.6529˚ and minimum is for 13H −C5−14H which is 107.1647˚. The dihedral angle is depends upon the structure of the molecule and compositions. The minimum value of dihedral angle was found to be 0.0575˚ in the clockwise direction for 16H−C7−C9−18H and the maximum value is 179.9831˚ for 21H−1O−C10−C9. Similarly, in anticlockwise direction maximum and minimum value of dihedral angles was found to be 179.8830˚ and 0.0487˚ respectively for C6−C8−C10−O1and 15H−C6−C8−17H.

Thermodynamic quantities (Ground state energy, Nuclear Repulsion Energy, Zero point Vibrational Energy, Thermal Energy, Specific Heat Capacity, and Entropy)

Table 2

Calculated Thermodynamic Quantities of Tyramine

Ground state energy (Hartree)	Nuclear Repulsion Energy (Hartree)	Zero point Vibrational Energy (Joules/ mol) or (kcal/mol)	Thermal Energy (kcal/mol)	Specific Heat Capacity (cal/ kol-Kelvin)	Entropy (cal/mol-Kelvin)
-438.8245	496.7198	469516.0 or 112.2170	118.2650	36.7570	96.7070

In the present study, some thermodynamic quantities like ground state energy, nuclear repulsion energy, zero point vibrational energy, thermal energy, specific heat capacity, entropy were calculated which are listed in the table 2 above. The ground state energy of title molecule was found to be -438.8245 Hartree. The lesser value of ground state energy shows the ground state stability of the molecule. Similarly, nuclear repulsion energy was found to be 496.7198Hartree. Also, the zero-point vibrational energy was also calculated and was 112.2170kcal/mol. The optimized value of thermal energy and entropy were found to be respectively 118.2650kcal/mol and 96.7070kcal/mol in DFT calculation.

Mulliken Atomic Charges

Mulliken atomic charges are useful in determining the chemical reactivity of compounds. The Mulliken charges of tyramine are listed in Table 3 below. C10 has the highest positive charge of all carbon atoms and thus predicted to be the target of nucleophilic attack on the title compound whereas nitrogen N2 has highest negative charge and thus predicted to be the target for electrophilic attack. Also, the atoms of oxygen atoms have a negative charge and all hydrogens have negative charges. The graphical representation of Mulliken charge versus atoms is represented in the figure 3 below.

Table 3

Mulliken Atomic Charges of Dopamine

Label number	Symbol	Mulliken Atomic Charge
1	O	-0.612814
2	N	-0.640994
3	C	-0.451609
4	C	0.025206
5	C	-0.213994
6	C	-0.188752
7	C	-0.191475
8	C	-0.224942
9	C	-0.179074
10	C	0.301764
11	H	0.185603
12	H	0.186313
13	H	0.203760
14	H	0.205356
15	H	0.179358
16	H	0.180965
27	H	0.171669
18	H	0.196737
19	H	0.254957
20	H	0.254485
21	H	0.357481

Figure 2

Plot of Mulliken Charge versus Atoms of Tyramine

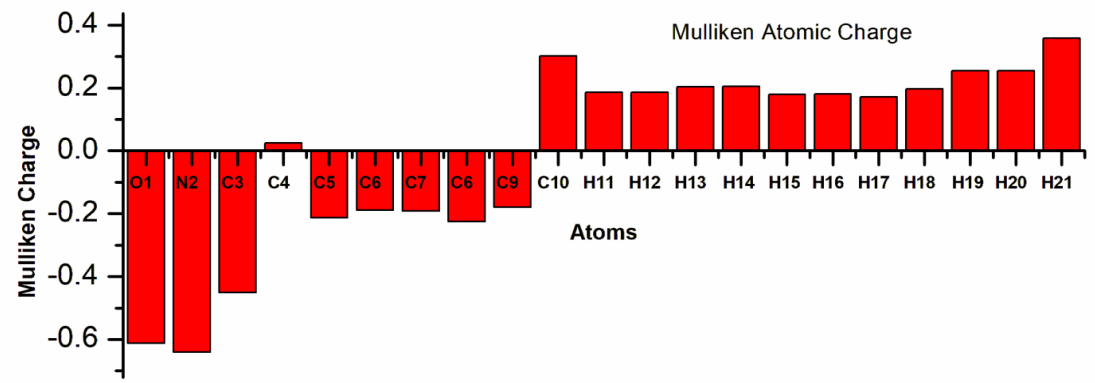

Vibrational Assignments

The tyramine consists of 21 atoms and thus gives 57 fundamental modes of vibration and is both Raman and IR active. The complete vibrational analysis of the 57 fundamental vibrational modes has been done by using DFT/B3LYP/6-21G. The optimized structural parameters were used in vibrational frequencies calculations to characterize all the stationary points as minima. The table 4 represents the calculated vibrational wave numbers, IR intensity, Raman activity and calculated PED for each normal mode. The PED assignments were given as per the internal coordinate system recommend by Pulay et al.. The theoretically predicted Raman and IR spectra are given in figures 2 and 4, respectively.

Table 4

Vibrational Wave Numbers, Raman Activity, IR Intensity and Potential Energy Distribution

Wavenumber		Raman Activity	IR intensity	Potential Energy Distribution (PED) ($\geq$5%)
Unscaled	Scaled			
48	48	2.8412	1.5661	R[δ(CCC)](8)+δ(N2C5C3)(72) +τ(C3C5)(18)
76	77	1.7491	1.0317	R[ω(CC)](35)+τ_a(18)]+$\delta_{sci}(CH_2)$(35)
101	102	0.0267	2.0869	τ(C3C5)(86)+δ(N2C5C3)(7)
204	206	0.1155	1.0679	R[τ_a(48) + oop(7)+[$\delta_{sci}(CH_2)$](30)
299	300	4.2128	41.8591	R[δ(C7C4C3)](36)+ρ(C8C10O)(11)]+τ(C3C5)(38)+γ (NC5H)(5)

314	316	6.8252	6.4151	R[δ_a(12)+ υ(C3C4)(12)]+δ_{sci}(CH_2)(54)+υ(C3C5)(7)
321	322	1.8173	18.4404	R[δ(CCC)(47)+ρ(C8C10O)(22)]+τ(C3C5)(12) +ρ(C5C3H)(5)
363	364	5.2478	144.2271	τ(CHO)(98)
394	394	5.0154	6.397	R[puck(25)+oop(CH)(17)+oop(13)+δ_a(5)]+ δ_{sci}(CH2)](19)
422	423	0.4753	9.2745	R[ρ(C8C10O)(48)+δ(CCC)(21)+δ'_a(15)]+τ(C3C5) (5)
442	443	0.0549	0.1076	R[τ'_a](84)
524	524	1.6439	3.4465	R[oop(CH)(33)+δ_a(22)+τ_a20)]+δ_{sci}($C5H_2$)(7)
572	572	0.4638	13.4553	R[oop(CH) (25)+τ_a(21)+δ_a(13) +oop(12)]+δ_{sci}($C3H_2$) (6)
679	677	5.5577	0.5974	R[δ'_a](81)
686	685	5.678	364.258	ω (NH_2)(68)+υ(CN)(20)
762	759	0.1171	1.4533	R[puck(55)+oop(C10H)(18)+υ(C3C4)(5)+δ_{trig}(5)]
769	766	0.2623	0.6066	ρ(NC5H)(44) +ρ(C5C3H)(30)+τ(C3C5)(15)
794	791	10.1522	10.609	R[puck(38)+δ_{trig}(9)+υ(C10O)(9)+υ(C3C4)(8)+ oop(CH)(15)]
847	842	9.2389	15.7594	R[oop(C8H)(45)+ω(CH)(42)
857	852	25.6167	11.214	R[δ_a](18)+υ(C10O)(11)+υ(CC)(26)+υ(C3C4) (9)+ω(CH)(17)+υ(C4C6)(7)]
870	865	5.8853	28.7301	R[oop(CH)(66)+τ_a(9)]+υ(CC)(6)
968	961	15.6384	47.8866	R[oop(CH)(44)+puck(7)]+υ(CC)(41)
977	969	0.781	0.5264	ρ(C5C3H)(33)+ρ(NH_2)(26)+ρ(NC5H) (22)+γ(NC5H)(10)
994	986	5.9508	8.8368	R[oop(CH)(63)+puck(8)+τ'_a(5)]+υ(CC)(11)
1007	1000	3.8654	2.7916	R[oop(CH)(72)+puck(15)]
1051	1043	0.26	0.0051	R[δ_{trig}(51)+υ(CC)(37)+ρ(CCH)(5)]
1084	1074	2.8607	9.3822	υ(CN)(76)+δ_{sc}(CH_2)(14)
1116	1105	2.5389	25.7994	R[υ(CC)(19)+υ(C3C4)(7)+ρ(C10C9H)(5)+δ(CHO) (6)]+γ(C5C3H)(18)+ρ(NH_2) 10)+γ(NC5H)(9)
1177	1164	5.8257	60.5742	R[ρ(CCH)(14)+υ(C7C9)(6)]+γ(C5C3H) (22)+δ(CHO)] (15) +ρ(NH_2)(9)+γ(NC5H) (9)+ρ(C5C3H)(5)
1189	1177	10.9438	165.377	R[υ(CO)(15)+ρ(C10C9H)(13)+υ(CC)(12)+υ(C6C8)(10)+δ (CHO)(32)]
1235	1221	33.8327	5.8984	R[υ(CC)(57)+δ_{trig}(14)+ρ(CCH)(8)+ρ(CCH)(7)]

1236	1222	3.445	3.7498	R[ρ(CCH) (71)+υ(CC)(20)]
1304	1287	3.2843	43.5099	R[υ(CO)(26)+υ(CC)(43)+δ_{trig}(7)]
1319	1302	4.2347	2.2015	R[ρ(CCH)(15)+υ(C10O)(7)+υ(CC)(16)]+ρ(NH_2)(14)+γ(C5C3H)(14)+ρ(NC5H)(11)+γ(NC5H)(8)
1329	1312	19.0785	0.894	R[υ(CC)](5) +ω(CH_2)(73)+ω(NC5H)(15)
1359	1340	4.5852	6.3067	R[υ(CC)(59)+ρ(CH_2)(7)]+γ(C5C3H)(15)+δ (CHO)(7)
1395	1376	22.9731	5.6159	ω(NC5H)(78)+ω(CH_2)(14)
1401	1382	5.2147	11.003	R[ρ(CCH)(58)]+γ(NC5H)(14)+ρ(NH_2)(9)+δ(CHO)(7) +γ(C5C3H)(5)
1404	1384	12.1846	6.0661	R[ρ(CCH)(15)]+γ(NC5H)(52)+ρ(NH_2)(17)
1484	1461	0.4156	27.6642	R[ρ(CCH)(35)+υ(CC)(33)+δ(CCC)(5)+ρ(CCO)(5)+δ(CHO)](9)+γ(C5C3H)(5)
1536	1511	34.9909	0.4315	δ_{sci}(CH_2)(95)
1551	1525	1.2681	6.5597	δ_{sci}(CH_2)(93)
1567	1540	7.2757	58.5786	R[ρ(CCH)(51)+υ(CC)(28)+υ(CO)(6)]
1616	1587	9.8491	12.6053	R[υ(CC)(62)+δ'$_a$(8) +ρ(CCH)(8)+δ(CHO)(5)]
1653	1623	52.3777	26.8625	R[υ(CC)(57)+δ_a(11)+ ρ(CCH)(18)]
1723	1689	15.7683	18.2191	δ_{sc}(NH_2)(96)
3038	2914	106.0159	24.481	υ_s(CH_2)(95)
3061	2935	31.8375	40.8058	υ_s(CH_2)(95)
3075	2947	86.9161	3.2757	υ_a(CH_2)(99)
3109	2979	9.8695	31.5707	υ_a(CH_2)(99)
3174	3037	58.511	15.5146	R[υ(CH)(99)]
3187	3049	41.6818	13.8475	R[υ(CH)(91)]
3194	3056	112.913	9.7735	R[υ(CH)(95)]
3230	3088	123.0748	4.2771	R[υ(CH)(95)]
3397	3238	126.1572	1.6921	υ_s (NH_2)(100)
3493	3324	68.2850	1.0009	υ_a(NH_2)(100)
3522	3350	172.903	19.7686	υ(OH)(100)

υ, stretching, δ, deformation, δ_{in}, in-plane deformation, oop, out-of-plane deformation, ω, wagging, ρ , rocking, γ, twisting, sc, scissoring and τ, torsion

Figure 3

IR Spectra of Tyramine between the Ranges 0 – 3400 cm^{-1}. Intensities of Selected Characteristics Modes are Assigned

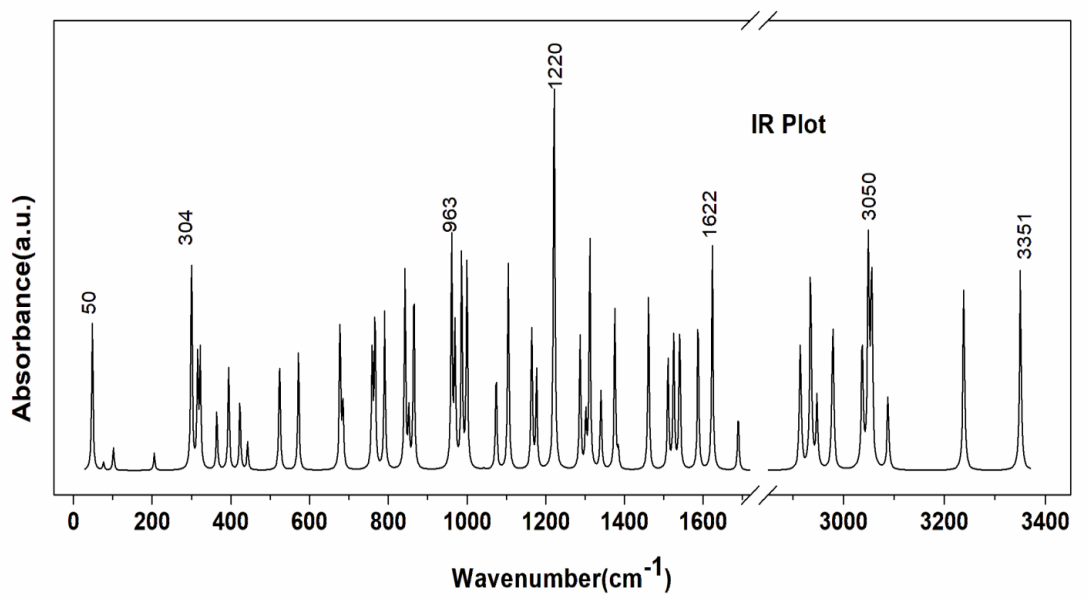

Figure 4

Raman Spectra of Tyramine between the Ranges 0 – 3360 cm^{-1}. Intensities of Selected Characteristics Modes are Assigned

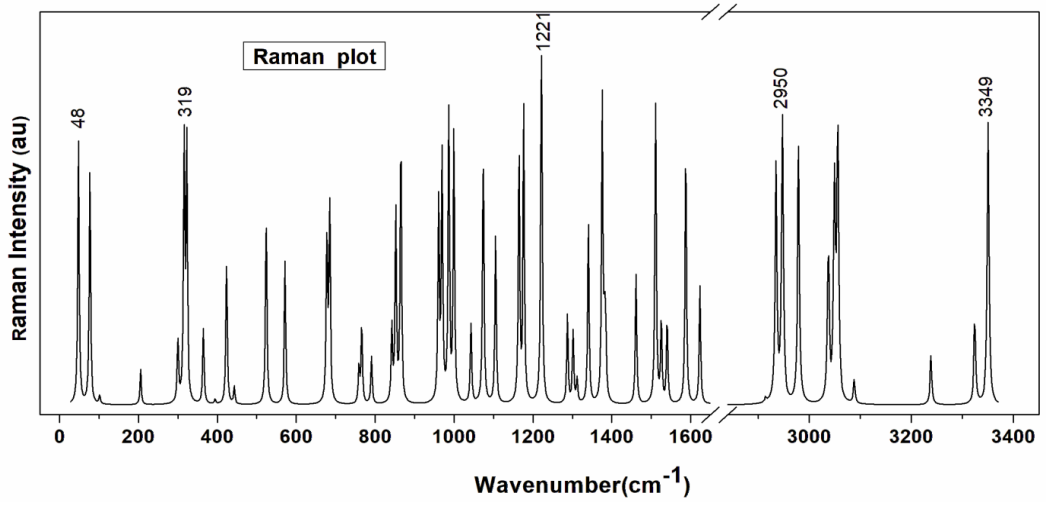

For a better discussion on calculated vibrational wavenumbers, the discussion is made according to the following sub-sections.

Phenyl Ring Vibration

Ring Vibration

Phenyl ring vibration includes C-C stretching, ring puckering, ring torsion, asymmetric deformation, asymmetric torsion and trigonal deformation. Generally, the strong C-C stretching vibrations are expected in the region of 1430-1650 cm^{-1} (Sathyanarayan, 2004). In this study, the C-C stretching vibrations ware calculated at 1623 and 1587 cm^{-1} with IR intensity/ Raman activity 26.8625/52.3777and 9.8491/12.6053 au respectively. Remaining C-C stretching vibrations ware also found which are respectively at 1221, 1222, 1287 and below 1116cm^{-1} as well. Trigonal ring deformation and ring puckering vibrations were recorded below 1287 and 1000 cm^{-1} respectively. Similarly, symmetric and asymmetric ring deformation vibrations were recorded below 572 and 676 cm^{-1} in scaled DFT. Also, ring twisting and rocking vibrations were recorded. They were found respectively below 1461 and 1623 cm^{-1} in scaled DFT.

C—H ***Vibration***

C—H vibration includes stretching, in-plane deformation and out-of-plane deformation modes which lie in the regions 3000-3100, 950-1450and 700-1000 cm^{-1} respectively (Joshi et al., 2018; Smith, 1999; Varsanyi, 1969). In this study, C-H stretching vibrations were calculated at 3037 cm^{-1} with IR intensity and Raman activity 15.5146 and 58.511 a.u. respectively. Other C-H stretching with higher PED contributions were calculated in the range 3049 cm^{-1} to 3088 cm^{-1} in the scaled frequency. In-plane bending and out of plane bending vibrations were recorded below 1623 and 1000 cm^{-1} in scaled DFT

O-H/COOH Vibration

The vibrations of hydroxyl group are likely to be the most sensitive to the environment i.e. it is free or hydrogen bonded. Thus, the hydrogen bonded species are associated with pronounced variation in the observables of a spectral band, like as band intensity and its shape, frequency position of band maxima. Free hydroxyl group absorbs strongly in the region 3600–3550 cm^{-1}, whereas hydrogen bond can lower the O-H stretching wavenumber to the 3550–3200 cm^{-1} region with an increase in IR intensity and breadth (Clothup et al., 1990). In this study, the pure mode (100% contribution in PED) in O-H stretching was calculated at 3350 cm^{-1} with Raman activity and IR intensity 172.903 and 19.7686 a.u. respectively. The CHO bending vibrations were calculated below 1587 cm^{-1}. And CO stretching vibrations were recorded in between 1540-1177 cm^{-1} in scaled DFT.

Ethyl Amine chain vibration

NH_2 group Vibration

NH_2 stretching vibration occurs in 3200-3450 cm^{-1} (Delabar & Majoube, 1978). In this study, pure NH_2 stretching modes were recorded at 3324 and 3238 cm^{-1} representing antisymmetric and symmetric stretching with IR intensity 1.0009, 1.6921units and Raman activity 68.285, 126.1572 units respectively. The in-plane bending of NH_2 group gives rise to its strong characteristic frequency in IR in the region 1550-1700 cm^{-1} and rocking modes the region 900-1150 cm^{-1} (Delabar & Majoube, 1978). In this study, the rocking modes were calculated below 1384 and scissoring vibrations were found at 1689 cm^{-1} with IR activity and Raman intensity respectively 18.219 and 15.7683 units in scaled DFT.

CH_2 Vibration

The asymmetric CH_2 stretching vibrations are generally observed in the region of 3000–2900 cm^{-1}, while the CH_2 symmetric stretch appears in the region 2900–2800 cm^{-1} (Balachandran & Pariman, 2012; Sajan et al., 2004). In the present study, CH_2 symmetric stretching were recorded at 2914, 2965 cm^{-1} with IR intensity/ Raman Activity 24.481/106.0159 and 40.8058/31.8375 units respectively. Also, asymmetric CH_2 stretching vibrations were calculated at 2947, 2979 cm^{-1} with IR intensity/ Raman Activity 3.2757/86.9161 and 31.5707/9.8695 units respectively in scaled DFT. CH_2 scissoring vibrations were recorded at 1511 and 1525 cm^{-1}. Also, wagging vibrations were recorded below 1376 cm^{-1}.

C-C-N chain Vibration

The C-N stretching frequency appears in the range 1000-1300 cm^{-1} for the amino derivatives of the benzene (Silverstein et al., 1981; Varsanyi, 1969). In the present study, C-N stretching vibration was measured at 1074, 685 cm^{-1} with IR intensity/ Raman Activity 9.3822/2.8607 and 364.258/5.6780 units respectively. C-C vibration was recorded at 979, 962 and 923 cm^{-1} with IR intensity/ Raman Activity 32.1348/15.3642, 30.9844/3.8491 and 6.771/10.6413 units respectively in scaled DFT. Twisting of CNH was recorded below 1383 cm^{-1} and rocking was below 1290 cm^{-1}. Torsion of C-C and that of C-N was recorded at 307 cm^{-1} with IR intensity 18.2397 units and Raman activity 2.1953 units in scaled DFT. C-C stretching bands were recorded below 986 and twisting of CNH were recorded below 1384 cm^{-1} in scaled DFT.

C4-C3 mode of Vibration

It is the linkage between phenyl ring and the ethyl amine moieties of the title compound. C4-C3 vibrations were found at 316, 852, 1105 cm^{-1} in scaled DFT.

Rocking and out-of-plane bending vibrations were recorded with lower value of PED (less than 5%).

Molecular Electrostatic Potential (MESP)

The molecular electrostatic potential (MESP) in a molecule at a point r (x,y,z) is the force on unitary positive test charge at that point due to its whole electrical charge and is given by following relation 3.2 (Joshi et al., 2021):

$$V(r) = \sum_{A} \frac{Z_A}{|\vec{R}_A - \vec{r}|} - \int \frac{\rho(\vec{r})dr}{|\vec{r}' - \vec{r}|} \quad (3.1)$$

Where, Z_A is the charge on nucleus A located at R_A and is the electron density. The first term is due to the nucleus and the second due to electron cloud.

In present study, molecular electrostatic potential (MESP) map has been mapped for tyramine as shown in Figure 5. The MESP is typically visualized through mapping its values onto the surface reflecting the molecule's boundaries. It correlates the total charge distribution with dipole moment, electronegativity, and partial charges and site of chemical reactivity of a molecule (Joshi & Chaudhary, 2013). The electrostatic potential (ESP) is a very much useful tool to understand the charge distribution within the molecules and it is used to scrutiny the variably charged regions of the molecule. Therefore, the distribution of charge within the molecule gives the information about the interaction of molecule with another molecule. The MESP is typically visualized through mapping its values onto the surface reflecting the molecule's boundaries. MESP provides a visual method to understand the relative polarity of a molecule and serves as a useful quantity to explain hydrogen bonding, reactivity and structure-activity relationship of molecules including biomolecules and drugs (Joshi & Chaudhary, 2013). In general the attractive potential appears in red colored regions and those of repulsive potential appear in blue. Negative electrostatic potential corresponds to an attraction of the proton by the concentrated electron density in the molecules (from lone pairs, pi-bonds, etc.). Positive electrostatic potential corresponds to repulsion of the proton by the atomic nuclei in regions where low electron density exists and the nuclear charge is incompletely shielded.

In the title compound, red (negative) region i.e. negative potential is located near nitrogen atom and little bit around oxygen whereas positive potential is located near the hydrogen of hydroxyl group. Also, the light yellow region in the benzene ring is the intermediate stage. The green region represents the area where ESP is zero. The potential increases in the order red < orange < yellow < green < blue (Khadka & Joshi, 2015). The negative region of MESP is responsible for the attraction of the proton.

Figure 5

Molecular Electrostatic Potential Surface Mapped between -6.608e-2 to 6.608e-2

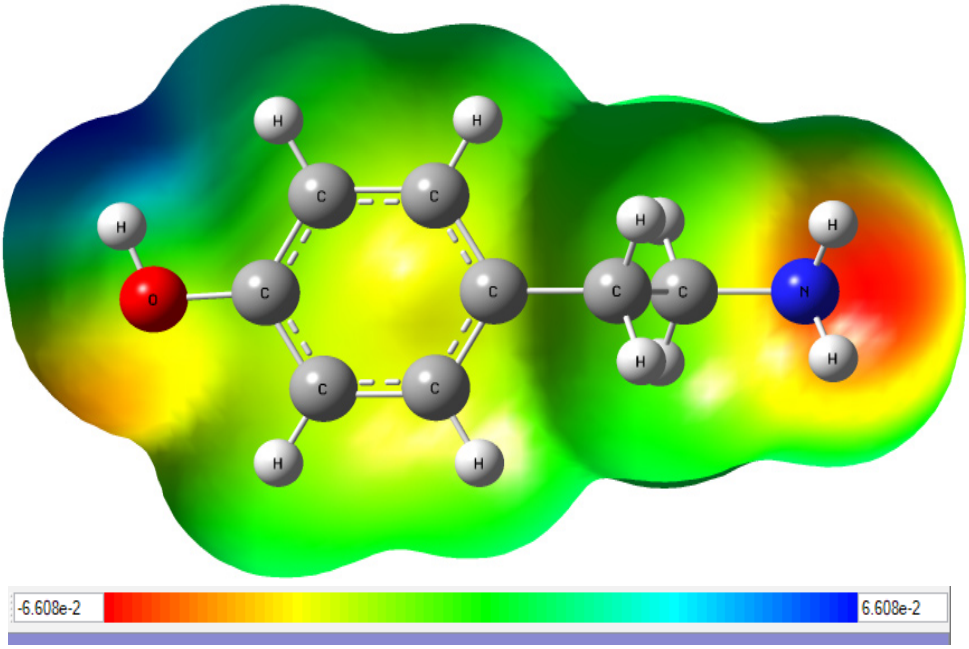

UV-Vis Spectral Analysis (HOMO-LUMO Energies, Absorption Wavelength, and Oscillator strength)

TD-DFT calculations were performed in both gaseous phase as well as solvent (water) environment in order to understand the electronic transitions in terms of energies and oscillator strength. Theoretically calculated absorption wavelength, energies and oscillator strength of tyrmine using TD-DFT and the chemical reactivity indices are represented in the table 5 (a). The calculated UV-Vis absorption spectra in gaseous and solvent phase are shown in the figures 6 and 7 respectively.

Table 5 (a)

Calculated Absorption Wavelength, Energies and Oscillator Strength of Dopamine using TD-DFT and Some other Quantities

S.N.	Transition states(Gas/Solvent)	Wavelength (nm)	Energy (eV)	Oscillator strength	Types of transition
1	H→L/ H→L	253.41/252.51	4.8927/ 4.9101	0.0224/0.0338	$\pi \rightarrow \pi^*$

2	H-1 →L/ H-1 →L	229.86/ 228.53	5.3940/ 5.4252	0.0156/ 0.0170	$\pi \rightarrow \pi^*$
3	H→L+1/ H→L+1	223.51/ 222.15	5.5472/ 5.5811	0.1491/ 0.1978	$\pi \rightarrow \pi^*$
4	H−1 →L+1/ H−1 →L+1	198.00/ 197.94	6.2617/ 6.2637	0.0512/ 0.0565	$\pi \rightarrow \pi^*$

Figure 6

UV Plot of Tyramine in Gas Phase between the Ranges 198-280cm^{-1}

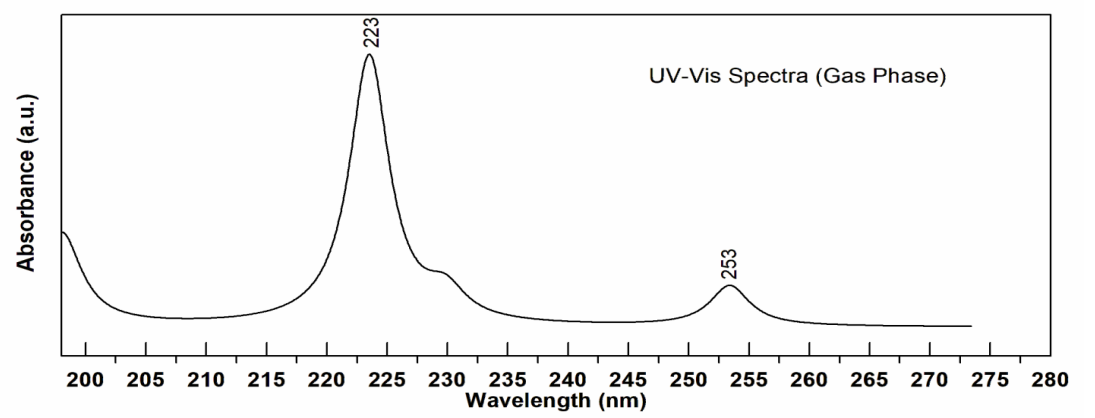

Figure 7

UV Plot of Tyramine in Solvent Phase between the Ranges 198-280cm^{-1}

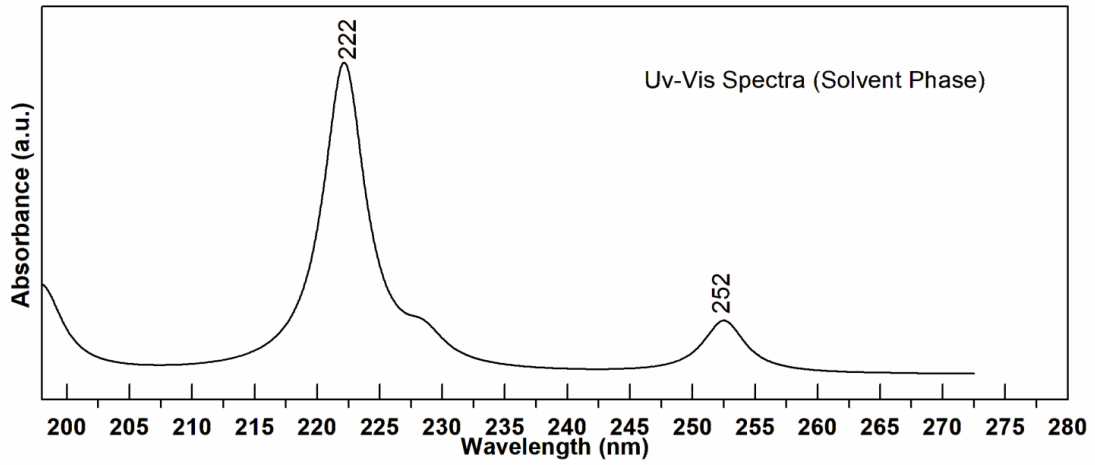

Highest occupied molecular orbital (HOMO) and Lowest unoccupied molecular orbital (LUMO) are those main orbitals which take part in chemical reactions. The energy difference between them is the key factor for determining the reactivity of the system. For clear understanding about electronic transition, positions

of theoretical absorption peaks, calculated wavelengths of corresponding transition, vertical excitation energy, and oscillator strengths were calculated for both gas phase and solvent environment which is presented in the table 5. It was found that the main dipole transition occurs at 253.41 nm (H→L) with oscillator strength 0.0224 and vertical excitation energy 4.8927 eV in gas phase whereas those values in solvent phase were 252.51nm, 0.0338and 4.9101 eV respectively. Another strong transition is H-1→L with wavelength 229.86 nm, oscillator strength 0.0156 with vertical excitation energy 5.3940 eV in gas phase and those values in solvent phase were 228.53nm, 0.0170 and 5.4252 eV respectively. Similarly, another strong transition (H →L+1) was found in both gas as well as solvent phase.

Electronegativity (χ), chemical potential (μ), global hardness (η), global softness (S) and global electrophilicity index (ω) can be calculated using the energies of frontier molecular orbitals E_{HOMO}, E_{LUMO} and given by relations 3.2-3.6 (Geerlimgs et al., 2003; Parr et. al., 1999) and these chemical reactivity indices are represented in the table 3.5 (b) below.

$$\chi = -\frac{1}{2}[E_{HOMO} + E_{LUMO}] \quad (3.2)$$

$$\mu = -\chi = \frac{1}{2}[E_{HOMO} + E_{LUMO}] \quad (3.3)$$

$$\eta = \frac{1}{2}[E_{LUMO} - E_{HOMO}] \quad (3.4)$$

$$S = \frac{1}{2}\eta \quad (3.5)$$

$$\omega = \frac{\mu^2}{2\eta} \quad (3.6)$$

Table 5(b)

Calculated Chemical Reactivity Indices Dopamine

↓Phase/Quantities→	E_{HOMO}	E_{LUMO}	ΔE	χ	μ	η	S	ω
Gas	-5.449	0.044	5.493	2.7025	-2.7025	2.7465	1.3732	1.35
Solvent (Ethanol)	-5.575	0.046	5.621	2.7645	-2.7645	2.8105	1.4052	1.36
Dipole Moment (Gas Phase)				Dipole Moment (Solvent Phase)				
2.0375 Debye				2.4574 Debye				

Energy of HOMO and LUMO state was calculated for both of the phase gas as well as solvent phase of tyramine. The HOMO and LUMO energy values were found to be -5.449 eV and 0.044 eV corresponding to gas phase as well as -5.575 eV and 0.046 eV corresponding to solvent phase respectively. Electronegativity (χ), chemical potential (μ), global hardness (η), global softness (S) and global

electrophilicity index (ω) value corresponding to gas phase were found to be 2.7025, -2.7025, 2.7465, 1.3732 and 1.35 eV respectively. Also, these values corresponding to solvent phase were found to be 2.7645, -2.7645, 2.8105, 1.4052and 1.36 eV respectively. The value of dipole moment corresponding to gas and solvent phase were 2.0375 and 2.4574 Debye respectively. The value of ΔE corresponding to gas and solvent phase are 5.493 and 5.621 eV respectively. The higher value of HOMO-LUMO gap suggests that the electronic transition occurs within the molecule from HOMO-LUMO. The HOMO-LUMO plots are given in the figure 8.

Figure 8

HOMO → LUMO Plot of Tyramine in Gas Phase

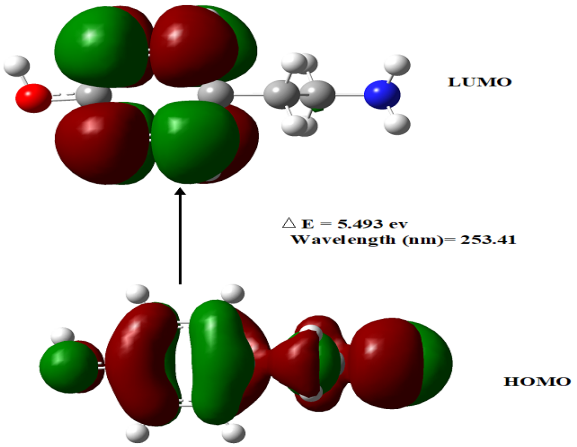

Molecular Docking Analysis

Molecular docking analysis is an excellent tool in drug design industry in order to understand the binding interactions among ligand and its protein (Joshi & Chaudhary, 2022). Docking calculations were reported using AutoDock Vina software. Trace amine-associated receptor 1 (1TQN) weas selected for docking. Some Docking parameters binding affinity, H-bonded residue and bond length of the title compound against these proteins were calculated.

Molecular Docking against Trace amine-associated Receptor 1 (1TQN)

Trace amine-associated receptor 1 **(**TAAR1) is widely distributed in the mammalian brain, particularly in limbic and monoaminergic areas. It is allegedly involved in mood, attention, memory, fear, and addiction. It also responds to a number of psychoactive drugs like amphetamines, ergoline derivatives, bromocriptine and lisuride (Rustigliano et al., 2018). Hence the molecular docking analysis has been performed to know the biological activities of tyramine with this

protein. The Ramachandran plot is represented in Figure 3.8 (a) demonstrate the phi-psi torsional angles of the residues of the protein. It shows that maximum residues lie inside the blue line which is the allowed region and thus suitable for docking. The docked structure is represented in the figures 3.8(b-e) and docking parameters are represented in the table 6 below.

Table 6

Docking Parameters of Tyramine against the Trace amine-associated Receptor 1

Protein	PDB code	Binding Affinity (kcal/mol)	H-Bonded Residue	Bond Length(Å)
Trace amine-associated receptor 1	1TQN	-6.0	A:ILE184	2.20
			A:ILE184	2.71

It was found that tyramine binds to the protein 1TQN of the protein with a binding affinity -6.0kcal/mol. The electropositive hydrogens (H20 and H19) in OH group interact non-covalently with residues A: ILE184 with bond length 2.20 Å and 2.71 Å respectively.

Figure 3.8 (a)

Ramachandran Plots of Protein 1TQN

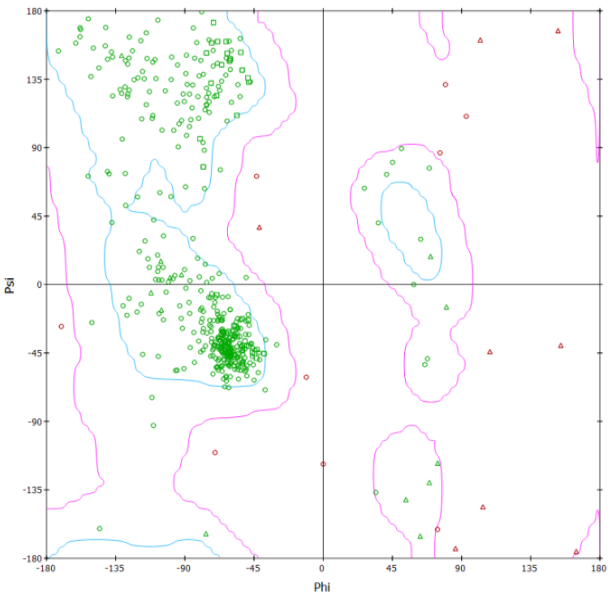

Figure 3.8 (b)

Interaction of Tyramine with Protein 1TQN(2D-View)

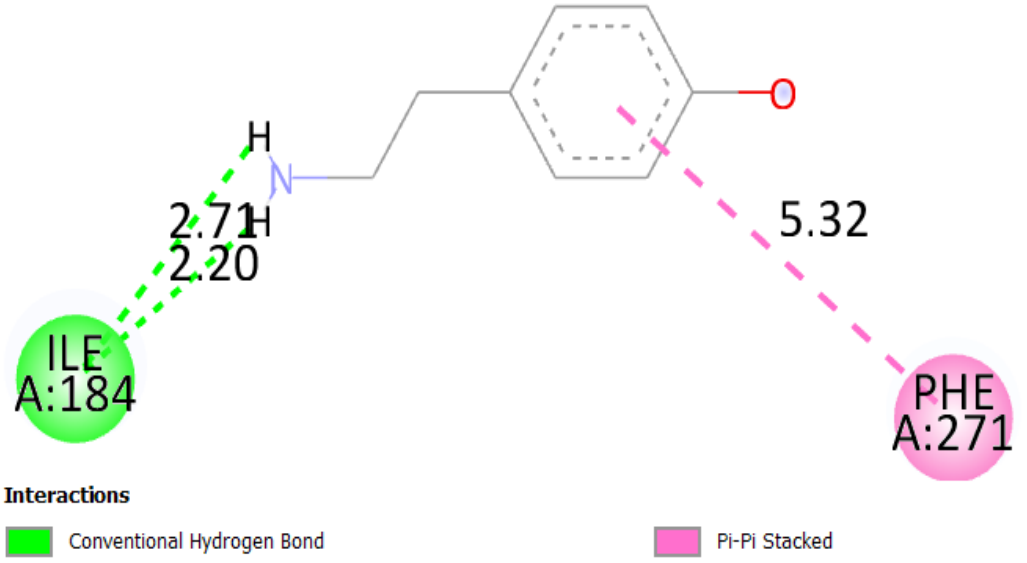

Figure 3.8 (c)

Interaction of Tyramine with Protein 1TQN(3D-View)

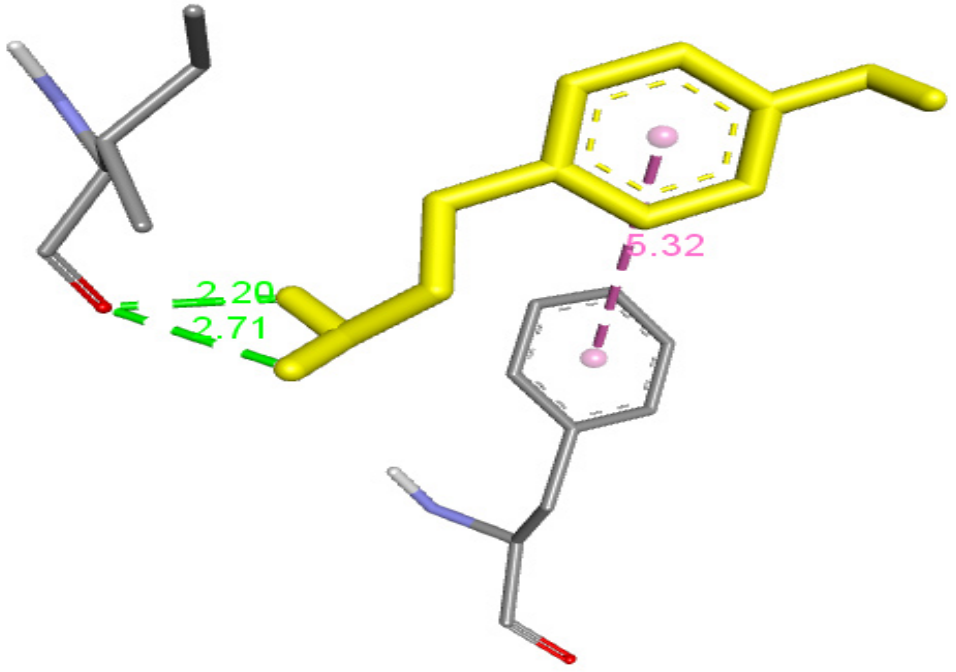

Figure 3.8 (d)

Docked Complex with Protein 1TQN

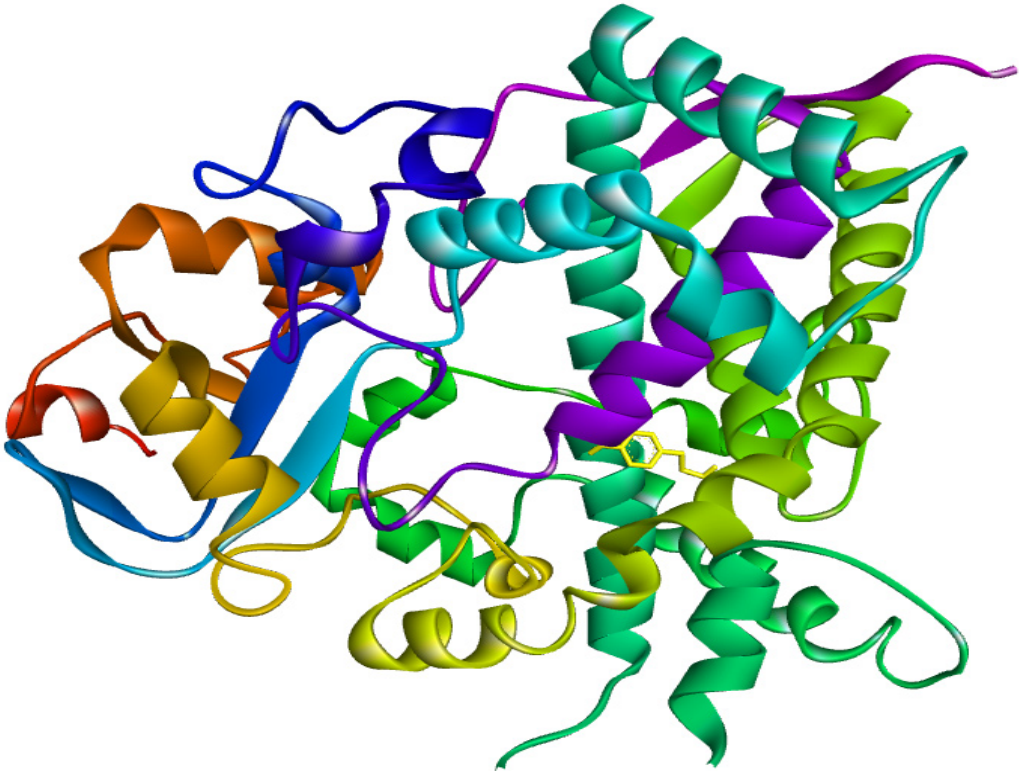

Figure 3.8 (e)

Docked Structure Showing Binding Pocket in Terms of H-Bond

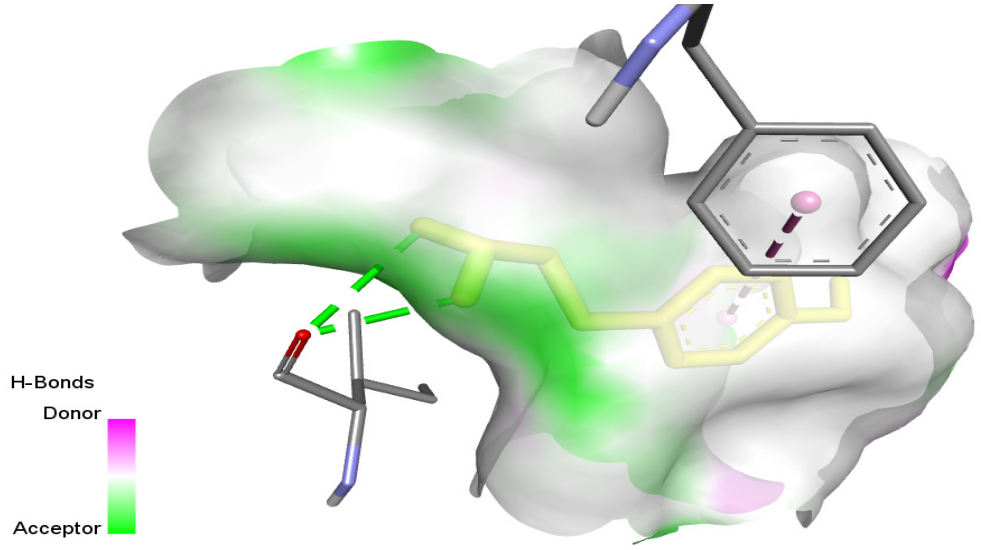

Conclusion

A computational study on structural, electronic, vibrational properties of tyramine using DFT and molecular docking study using AutoDock Vina has been conducted to study molecular structure, vibrational frequency analysis, MEP, HOMO-LUMO analysis and molecular docking of the title compound. All the calculated vibrational modes were found to be both IR and Raman active. From MEP mapping, basic and key information regarding to the size, shape, charge density distribution and sites of chemical reactivity of the title molecule has been fetched out. Negative potential is found to be located near nitrogen atom whereas positive potential is located near the hydrogen (H21) of hydroxyl group. Also, the light yellow region in benzene ring was predicted as an intermediate stage.

The electronic transition has been calculated in the gas phase as well as in ethanol environment (solvent) using TD-DFT/B3LYP/6-21G basis set shows the charge transfer within the molecule. HOMO-LUMO made very clearly the involvement of charge transfer between the donor and acceptor groups. The band gap (5.493 eV) in gaseous phase phase between these two frontier energy levels shows its stability. Furthermore, the binding sites of the title molecule and the protein matrix have been predicted. The binding affinity of the protein (Trace amine-associated receptor 1)-molecule complex was predicted to be −6.0 kcal/mol. Thus, the molecular docking study theoretically proves that the title molecule has a good binding potential against the protein Trace amine-associated receptor 1 (1TQN) Showing the importance of title molecule chemical biology, Pharmacology, medicinal chemistry and drug designing fields to develop new drugs and materials.

References

Balachandran, V., & Parimala, K. (2012). Molecular structure, vibrational spectra, NBO analysis, first hyperpolarizability, and HOMO, LUMO studies of mesityl chloride by density functional methods. *Journal of Molecular Structure*, *1007*, 136-145.

Becke, A. D. (1993). Prospective on "density-functional thermochemistry III. The role of exact exchange. *Journal of Chemical Physics*, 98, 5648–5652.

Broadley, K. J. (2010). The vascular effects of trace amines and amphetamines. *Pharmacology & Therapeutics*, *125*(3), 363–375.

Burchett, S. A., & Hicks, T. P. (2006). The mysterious trace amines: Protean neuromodulators of synaptic transmission in mammalian brain. *Progress in Neurobiology*, *79*(5–6), 223–246.

Casida, M. E., Casida, K. C., & Salahub, D. R. (1998). Excited-state potential energy curves from time-dependent density-functional theory: A cross section of formaldehyde's $^1A_1$ manifold. *International Journal of Quantum Chemistry*, *70*(4-5), 933–941.

Chaudhary, T., & Joshi, B. D. (2022). Electronic, thermodynamic properties, nonlinear optical responses, and molecular docking studies on cephalexin. *Journal of Institute of Science and Technology, 27*(1), 83–92.

Chong, D.P. (1995). *Recent advances in density functional methods.* Singapore World Scientific.

Clothup, N.B., Daly, L.H., & Wiberley, S.E. (1990). *Introduction to infrared and raman spectroscopy*. Academic Press.

Corminboeuf, C., Tran, F., & Weber, J. (2006). The role of density functional theory in chemistry: Some historical landmarks and application to zeolites. *Journal of Molecular Structure: THEOCHEM, 762*(1-3), 1–7.

Cruickshank, L., Kennedy, A. R., & Shankland, N. (2013). Tautomeric and ionisation forms of dopamine and tyramine in the solid state. *Journal of Molecular Structure*, 1051, 132–136.

Crupi, V., Majolino, D., Mondello, M.R., Migliardo, P., & Venuti, V. (2002). FT-IR spectroscopy: A powerful tool in pharmacology. *Journal of Pharmaceutical and Biomedical Analysis*, *29*(6), 1149–1152.

Delabar, J. M., & Majoube, M. (1978). Infrared and raman spectroscopic study of 15N and D- substituted guanines. *Spectrochimica Acta Part A*, *34*(2), 129–140.

Dewar, M.J.S., & Schmeising, H.N. (1960). Resonance and conjugation –II factors determining bond lengths and heats of formation. *Tetrahedron*, *11*(1-2), 96 – 120.

Dong, C., Shi, S., Pan, N., Du, X., Li, H., & Xia, X. (2022). Inhibitory mechanism of tyramine-degrading strains on reducing tyramine accumulation in Harbin dry sausage during fermentation. *Food Control*, 137: 108952.

Fini, G. (2004). Applications of raman spectroscopy to pharmacy. *Journal of Raman Spectroscopy, 35*, 335-337.

Frisch, M.J., Trucks, G.W., Schlegel, H.B., Scuseria, G.E., Cheeseman, J.R., Robb, M.A., … & Fox, D. J. (2010). *GAUSSIAN 09, Revision*. Gaussian, Inc., Wallingford CT.

Frish, A., Nielson A. B., & Holder, A. J. (2009). *Gauss view user manual.* Gaussian Inc, Pittsburgh, P.A.

Hohenberg, P., & Kohn, W. (1964). Inhomogeneous electron gas. *Physical Journal review, 136*(3B), 864-871.

Joshi B. D., & Chaudhary, P. N. (2013). Molecular structure, MESP, HOMO-LUMO and vibrational analysis of β-Asarone using density functional theory. *Kathmandu University Journal of Science, Engineering and Technolgy, 9*(2), 1–14.

Joshi, B. D., Srivastava, A., Tondon, P., Jain, S., & Ayla, A. (2018). A combined experimental (IR, Ra,an and UV-Vis) and quantum chemical study of canadine. *Spectrochimica Acta Part A*, 1991, 249–258.

Joshi, B. D., Thakur, G., & Chaudhary, M. K. (2021). Molecular structure, HOMO –LUMO and vibratiinal analysis of ergoline by density functional theory. *Scientific World*, *14*(14), 21–30.

Khadka, J. B., & Joshi, B. D. (2015). Molecular electrostatic potential, HOMO-LUMO and vibrational study of aristcholochic acid III using density functional theory. *BIBECHANA*, 12, 40–52.

Kohn, W., & Vashishta, P. (1983). *"General Density Functional Theory" in theory of the inhomogeneous electron gas*. S. Lundqvist & N.H. March (Eds.). Plenum, New York.

Lee. C. T., Yamg, W., & Parr, R. G. (1988). Development of the colle-salvetti correlation-energy formula into a functional of the electron density. *The Journal of Physical Chemistry* B, 37, 785–789.

Lindemann, L., & Hoener, M. C. (2005). Technical peculiarities of targeting TAARs in drug development: A renaissance in trace amines inspired by a novel GPCR Family. *Trends in Pharmacological Sciences*, *26*(5), 274–281.

Martin, J.M. L., & Alsenoy, C. V. (1995). *Gar2ped*. University of Antwerp.

Misra, R., Joshi, B. D., Srivastava, A., Tondon, P., & Jain, S. (2014). Quantum chemical and experimental studies on the structure and vibrational spectra of an alkoid- corlumine. *Spectrochimica Acta Pat A,* 118, 470–480.

Morris, G. M., Huey, R., Lindstrom, W., Sanner, M.F., Belew, R.K., & Goodsell D. S. (2009). AutoDock4 and AutoDock Tools4: Automated docking with selective receptor flexibity. *Journal of Computational Chemistry*, *30*(16), 2785–2791.

Panas, M. W., Xie, Z., Panas, H.N., Hoener, M. C., Vallender, E. J., & Miller, G. M. (2012). Trace amine associated receptor 1 signaling in activated lymphocytes. *Journal of Neuroimmune Pharmacol*ogy, *7*(4), 866–876.

Parr, R.G., Szentpaly, L., & Liu, S. (1999). Electropholicity index. *Journal of American Chemical Society, 121*(9), 1922–1924.

Podder, A., Dattagupta, J. K., Saha, N. N., & Saenger, W. (1979). Crystal and molecular structure of a symparthomimetic amine, tyramine hydrochloride. *Acta Crystallographica Section B. B35*, 649–652.

Pouling, L. (1960). *The nature of the chemical bond.* Cornell Univ. Press.

Pulay, P., Foragasi, G., Pang, F., & Boggs, J. E. (1979). Systematic ab initio gradient calculation of molecular geometries, force constants, and dipole moment derivatives. *Journal of American Chemical Society*, *101*(10), 2550–2560.

Quevedo, R., Nuñez-Dallos, N., Wurst, K., & Duarte-Ruiz, Á. (2012). A structural study of the intermolecular interactions of tyramine in the solid state and in solution. *Journal of Molecular Structure*, 1029, 175–179.

Rafehi M., Faltraco F., Matthaei J., Prukop T., Jensen O., Grytzmann A., Blome F.G., Berger R.G., Krings U., Vormfelde S.V., Tzvetkov M.V., & Brockmöller J. (2019). Highly variable pharmacokinetics of tyramine in humans and polymorphisms in OCT1, CYP2D6, and MAO-A. *Front. Pharmacol,* 10, 1297.

Sajan, D., Binoy, J., Pradeep, B., Krishna, K. V., Kartha, V. B., Joe, I. H., & Jayakumar, V. S. (2004). NIR-FT raman and infrared spectra and ab initio computations of glycinium oxalate. *Spectrochimica Acta Part A*, *60*(1-2), 173–180.

Salter, M., & Kenney, A. (2018) Myocardial injury from tranylcypromine-induced hypertensive crisis secondary to excessive tyramine intake. *Cardiovascular Toxicol*ogy, *18*, 583–586.

Sathyanarayan, D. N. (2004). *Vibrational spectroscopy: Theory and applications.* New Age International.

Schrödinger, LLc, & PyMOl, D. W. (2020). *The PyMOL molecular graphics system, Version 2.5.4*.

Siddiqui, S. A., Dwivedi, A., Singh, P. K., Hasan, T., Jain, S., Sundaraganeshan, N., Saleem, H., & Misra, N. (2009). Vibrational dynamics and potential energy distribution of two well-known neurotransmitter receptors: Tyramine

and dopamine hydrochloride. *Journal of Theoretical and Computational Chemistry*, *8*(3), 433–450.

Silverstein M., Basseler, G. C, & Morill, C. (1981). *Spectometric identification of organic compounds.* Wiley.

Smith, B. (1999). *Infrared spectral interpretation: A systematic approach.* CRC Press.

Systemes, D. (2016). *BIOVIA Discovery Studio Dassault Systmes*.

Trott, O., & Olson, A. J. (2010). AutoDock Vina: Improving the speed and accuracy of docking with a new scoring function, efficient optimization and multithreading, *Journal of Computational Chemistry*, 31, 455-461.

Ullah, H., Shah, A. A, Ayub, K., & Bilal, S. (2013). Density functional theory study of poly(*o*-phenylenediamine) oligomers**.** *The Journal of Physical Chemistry C*, *117*(8), 4069–4078.

Varsanyi, G. (1969). *Vibrational Spectra of Benzene Derivatives*. Academic Press.

Yadav, T., & Mukherjee,V. (2017). Structural modeling and spectroscopic investigation of isolated and hydrochloride tyramine neurotransmitter. *Journal of Molecular Structure, 1147*, 702–713.